A R C H I V E O F M E C H A N I C A L E N G I N E E R I N G

VOL. LXV 2018 Number 3

DOI: 10.24425/124484

Key words: Monte Carlo, SERPENT, AP1000, PWR, nuclear reactor

PIOTR DARNOWSKI[1], *PATRYK IGNACZAK*[1], *PAWEŁ OBRĘBSKI*[1], *MICHAŁ STĘPIEŃ*[1], *GRZEGORZ NIEWIŃSKI*[1]

SIMULATIONS OF THE AP1000-BASED REACTOR CORE WITH SERPENT COMPUTER CODE

The paper presents the core design, model development and results of the neutron transport simulations of the large Pressurized Water Reactor based on the AP1000 design. The SERPENT 2.1.29 Monte Carlo reactor physics computer code with ENDF/B-VII and JEFF 3.1.1 nuclear data libraries was applied. The full-core 3D models were developed according to the available Design Control Documentation and the literature. Criticality simulations were performed for the core at the Beginning of Life state for Cold Shutdown, Hot Zero Power and Full Power conditions. Selected core parameters were investigated and compared with the design data: effective multiplication factors, boron concentrations, control rod worth, reactivity coefficients and radial power distributions. Acceptable agreement between design data and simulations was obtained, confirming the validity of the model and applied methodology.

1. Introduction

Currently, there are 447 (01.09.2017) nuclear power reactors, which are operated in 31 countries in the World. Their total installed capacity exceeds 392.3 GWe, and they provide 10.6% of the world's electricity. There are also 56 nuclear reactors under construction, which will eventually supply the total installed capacity with additional 60.6 GWe. In addition, many countries plan to build another 351 nuclear power reactors in the future [1, 2].

Nowadays, many forecasts predict a relevant increase of the future energy consumption. According to the Energy Outlook 2016 [3], electric power generation will increase by an average of 1.2%/year from 2012 to 2040. It is predicted that the electricity generation from nuclear power worldwide will increase from 2300 TWh in 2012 to 4500 TWh in 2040 [3]. It means that the total installed nuclear capacity

[1] *Institute of Heat Engineering, Warsaw University of Technology, Nowowiejska 21/25, 00-665 Warsaw, Poland. Emails: piotr.darnowski@itc.pw.edu.pl, patryk.ignac@gmail.com, obrebski.pawel@gmail.com, michal.stepien@itc.pw.edu.pl, grzegorz.niewinski@itc.pw.edu.pl*

is forecasted to grow. The leader in nuclear investments in non-OECD countries is China, which prospected addition of 139 GWe nuclear capacity till 2040. In OECD countries, the first place belongs to South Korea with 15 GWe. There are some states whose nuclear capacity is planned to be reduced, for instance, Canada, Japan and OECD Europe [3]. Nevertheless, the main advantages of nuclear power, which can be undoubtedly called as incentives for investment in this field is practically no greenhouse gas emissions, high capacity factor, stable and low fuel prices and highly developed technology of modern designs [1–3].

Nuclear power plants (NPP) are considered as one of the possible solutions to diversify Polish energy mix, where the coal is playing a dominant role with electricity production share equal to 88% in 2012 [4]. According to EU Policy and regulations, reduction of CO_2 emission, by decreasing the share of the coal-fired fleet is a target, which can be achieved or supported by the nuclear program.

The potential construction of the first NPP in Poland, as well as constant need of research and development in the scope of the nuclear reactors safety, became the primary motivation for this work. The first task of this work was to develop Monte Carlo numerical model of the nuclear reactor core based on the Westinghouse AP1000 design. The model was developed applying publicly available reports – especially official Design Control Document (DCD) submitted by the designer to the US Nuclear Regulatory Commission (NRC) [5–10]. In consequence, the core model developed in this work should be considered as AP1000 based or "like" design. The second aim of this work was to test and validate the model and the methodology, using neutronic simulations of selected core parameters. Worth to mention that the AP1000 design is one of the potential technologies considered for the first Polish NPP.

The AP1000 is the Pressurized Water Reactor (PWR) classified as generation III+ design. It is considered as an advanced and inherently safe modern design with passive safety philosophy applied as far as possible. In comparison to the III generation reactors, it has also more simplified, modular design, which enhances its potential construction time and makes it more economically effective. The Nuclear Power Plant with AP1000 reactor consists of a two-loop Reactor Coolant System with 3415 MWth gross thermal power and 1110 MWe of a nominal net electrical output [6, 11]. The typical core fuel cycle is anticipated to take 12–18 months between refuelling. The maximum average burnup, which is approved by the US NRC, is 60 GWd/MTU (GigaWatt days per metric tonne of uranium) [8, 11].

2. Materials, geometry and modelling

2.1. SERPENT computer code

The SERPENT is a continuous energy neutron transport Monte Carlo computer code which has been developed by Finnish VTT research centre since 2004 [12–14]. The code was used as a State-of-the-Art Monte Carlo tool for Reactor Physics

applications with fuel burnup capability. The code and Monte Carlo method were applied as an excellent tool to study the neutronics of complex nuclear systems. In order to perform simulations, the proper input files had to be prepared. This required a precise definition of the model, including design, geometry definition, all materials in the core and additional code setup. Input files were divided into different cases to analyse various parameters. Initially, the 2D model was developed, as it was more straightforward and computationally effective, then it was extended to the 3D model. In this paper, only 3D results are reported.

2.2. Materials

First of all, it was necessary to determine required materials which are used in the core design. The list of those materials was prepared according to the literature and reactor's DCD [8]. All these materials were defined regarding SERPENT material cards. In order to define material for nuclear design, knowledge about the total atomic or mass density is necessary, and knowledge of weight fractions, atomic fractions or atomic number densities of all isotopes. The primary material composition estimation methodology was based on the approach presented in references [15, 16]. For all materials, temperatures were specified to assign proper cross sections (reaction probabilities) from temperature-dependent nuclear data libraries, Doppler broadening and thermal-scattering SERPENT procedures [17]. The core model developed in this work considers only the fresh core at the Beginning of Life (BOL). In consequence, there is no burnup effect on the materials.

2.2.1. Uranium dioxide

The fuel is made of uranium dioxide (UO_2) which has the form of sintered fuel pellets with a density equal to 10.4668 g/cm^3, and it is 95.5% of theoretical density of 10.96 g/cm^3 [6, 18, 19]. There are five distinct U-235 isotope enrichments: 1.58%, 2.35%, 3.2%, 3.4%, 4.45% [8]. The three oxygen isotopes: O-16, O-17, and O-18 were calculated, but the O-18 was not available in the nuclear data libraries and was exchanged to O-16. A similar approach was applied to oxygen in the water. Moreover, it was necessary to estimate the U-234 content, and it was assumed to be 0.8 wt% of U-235 [15]. Additional reduced compositions without O-17 and U-234 were prepared for sensitivity calculations. Those were prepared as some analyses do not consider those isotopes [20]. Sensitivity simulations were also prepared for 10.97 g/cm^3 and 10.98 g/cm^3 as different values are possible to find in the literature. In general, AP-1000 DCD [8] does not specify detailed material compositions and estimations were necessary. The atomic number densities for the fuel are presented in Table 1. Small differences between number densities are present due to the assumed constant fuel density and slightly changing average atomic mass.

Table 1.

The fuel material atomic number densities (for UO_2 95.5% TD = 10.96 g/cm^3)

Isotope	Enrichment [wt% U-235]				
	1.58 wt%	2.35 wt%	3.2 wt%	3.4 wt%	4.45 wt%
	Atomic density [atoms/barn-cm]				
Composition without simplifications					
U-234	3.00079049E–06	4.46314840E–06	6.07739953E–06	6.45721721E–06	8.45122188E–06
U-235	3.73498192E–04	5.55512910E–04	7.56433261E–04	8.03707877E–04	1.05189486E–03
U-238	2.29688057E–02	2.27873770E–02	2.25871035E–02	2.25399811E–02	2.22925932E–02
O-16	4.66728670E–02	4.66769622E–02	4.66814827E–02	4.66825463E–02	4.66881303E–02
O-17	1.77424316E–05	1.77439883E–05	1.77457068E–05	1.77461111E–05	1.77482338E–05
Reduced composition without O-17					
U-234	3.00079049E–06	4.46314840E–06	6.07739953E–06	6.45721721E–06	8.45122188E–06
U-235	3.73498192E–04	5.55512910E–04	7.56433261E–04	8.03707877E–04	1.05189486E–03
U-238	2.29688057E–02	2.27873770E–02	2.25871035E–02	2.25399811E–02	2.22925932E–02
O-16	4.66906095E–02	4.66947062E–02	4.66992284E–02	4.67002924E–02	4.67058785E–02
Reduced composition without U-234 and O-17					
U-235	3.73498288E–04	5.55513122E–04	7.56433654E–04	8.03708321E–04	1.05189562E–03
U-238	2.29717619E–02	2.27917737E–02	2.25930903E–02	2.25463420E–02	2.23009181E–02
O-16	4.66905203E–02	4.66945736E–02	4.66990479E–02	4.67001007E–02	4.67056275E–02

2.2.2. Integral Fuel Burnable Absorber

Integral Fuel Burnable Absorber (IFBA) are neutron absorbers used during the initial part of the cycle to compensate for the excess reactivity and to control reactor peaking factors. Together with discrete burnable absorbers, they prevent moderator temperature coefficient from being positive for normal operation of the reactor [8]. At the beginning of the cycle, they reduce the required soluble boron concentration in the water, and they fade with a burnup time until they get burned out. The IFBA pellets are UO_2 pellets covered by absorbing material with a thickness equal to about ~0.001 inches (0.00254 cm) [7]. According to [8], a thin coating of ZrB_2 material, with 0.772 mg/cm of B-10 content was used for the 1st

Table 2.

IFBA material composition [20]

Isotope	Weight fraction [–]
B-10	0.0187
B-11	0.1713
Zr–90	0.416745
Zr–91	0.090882
Zr–92	0.138915
Zr–94	0.140778
Zr–96	0.02268

cycle core. The natural isotopic composition of the zirconium diboride ZrB_2 was applied. The coating density was selected to be 5.42 g/cm^{3,} and IFBA geometry was used the same as in Ames model [20]. Worth to mention that different values are also available in the literature [21].

2.2.3. Borosilicate burnable absorbers

Pyrex rods serve as discrete burnable absorbers (BP or BAs). They consist of neutron-absorbing borosilicate glass tubes (B_2O_3–SiO_2). Their function is similar to the IFBAs – they control the excess reactivity for the initial part of the first cycle. According to [8], borosilicate glass rods in AP1000 reactor have 6.24 mg/cm of B-10 content and use 12.5 wt% of B_2O_3. A detailed description of Westinghouse BP Pyrex rods is available in [22]. The material has a density equal to 2.299 g/cm^3, and its composition is defined in Table 3 [22].

Table 3.

Pyrex (borosilicate glass) rods material card [22]

Element or isotope	Weight fraction [–]
B-10	0.00699
B-11	0.03207
O	0.53902
Al	0.01167
Si	0.37856
K	0.00332
Na	0.02837

2.2.4. Cladding

The ZIRLO™ is the zirconium alloy material designed by Westinghouse, which is a modification of Zircaloy-4 alloy with the addition of Niobium. It is used as a structural material for fuel cladding, instrumentation and guide tubes. The reference [25] discuss the limitations onto the material's chemical composition, but in general, the precise composition is not publicly available. The composition of the optimized ZIRLO variant presented in Table 4 was applied, and it is based

Table 4.

Optimized ZIRLO™ material card [26, 27]

Element	Weight fraction [–]
Sn	0.0067
Fe	0.001
Nb	0.01
O	0.0012
Zr	0.9811

on reference [26]. The composition consists of naturally occurring elements [27]. The density of ZIRLO was assumed to be the same as Zircaloy-4 and equal to 6.55 g/cm^3 [15].

2.2.5. Ag–In–Cd – a neutron absorber

Ag–In–Cd (Silver–Indium–Cadmium) is a chemical compound used as a neutron absorber in Gray Rod Control Assembly (GRCA) and Rod Cluster Control Assembly (RCCA). The applied density of this material is 10.159 g/cm^3 [8], and isotopic composition [15] is presented in Table 5.

Table 5.

Ag–In–Cd material atomic number densities [15]

Isotope	Atomic Density [atom/b-cm]
Ag–107	2.3523E–02
Ag–109	2.1854E–02
In–113	3.4291E–04
In–115	7.6504E–03
Cd–106	3.4019E–05
Cd–108	2.4221E–05
Cd–110	3.3991E–04
Cd–111	3.4835E–04
Cd-112	6.5669E–04
Cd–113	3.3257E–04
Cd–114	7.8188E–04
Cd–116	2.0384E–04

2.2.6. Structural steels

Two types of steel were considered in the model. The first is Type 304 SS (Stainless Steel), and it is a structural material used for claddings in RCCAs, GRCAs and Pyrex rods. It also serves as a surrogate of a neutron absorber material in 12 out of 24 gray rods in GRCAs [8]. The material was used in the reactor's core shroud and core barrel, as well [28]. The density of SS-304 was assumed to be 7.889 g/cm^3 [17], and its composition, along with atomic densities of isotopes were found in [15] and presented in Table 6.

The second steel is SA-508 Cl. 3, and it is low carbon steel, which is used as a structural material for the reactor pressure vessel [29]. The density of typical carbon steel equal to 7.85 g/cm^3 was applied [30]. The chemical composition of this material was found in [31] and is shown in Table 7.

Table 6.

Stainless Steel Type 304 number densities

Isotope	Number density [atom/b-cm]
Si-28	9.5274E–04
Si-29	4.8400E–05
Si-30	3.1943E–05
Cr-50	7.6778E–04
Cr-52	1.4806E–02
Cr-53	1.6789E–03
Cr-54	4.1791E–04
Mn-55	1.7604E–03
Fe-54	3.4620E–03
Fe-56	5.4345E–02
Fe-57	1.2551E–03
Fe-58	1.6703E–04
Ni-58	5.6089E–03
Ni-60	2.1605E–03
Ni-61	9.3917E–05
Ni-62	2.9945E–04
Ni-64	7.6261E–05

Table 7.

Low carbon SA-508 Cl. 3 steel material card [31]

Element	Weight fraction [–]
C	0.0019
Si	0.0008
Mn	0.0135
P	0.00006
S	0.00002
Ni	0.0082
Cr	0.0017
Mo	0.0051
Fe	0.96872

2.2.7. Inconel-718

Inconel-718 is an alloy used as construction material for mixing spacer grids. The composition is presented in Table 8 for density equal to 8.2 g/cm^3 [15].

Table 8.

Low carbon SA-508 Cl. 3 steel material card [15]

Isotope	Number density [atom/b-cm]
Si-28	5.6753E–04
Si-29	2.8831E–05
Si-30	1.9028E–05
Cr-50	7.8239E–04
Cr-52	1.5088E–02
Cr-53	1.7108E–03
Cr-54	4.2586E–04
Mn-55	7.8201E–04
Fe-54	1.4797E–03
Fe-56	2.3229E–02
Fe-57	5.3645E–04
Fe-58	7.1392E–05
Ni-58	2.9320E–02
Ni-60	1.1294E–02
Ni-61	4.9094E–04
Ni-62	1.5653E–03
Ni-64	3.9864E–04

2.2.8. Borated water

Light water (H_2O) serves as a coolant and moderator in a PWR reactor. It is pressurized to ~155 bar, and its temperature is in the range of 260–315°C for hot conditions [6]. The water densities were recalculated with IAPWS-IF97 implementation X-Steam for Matlab environment [32] for the cold shutdown, hot zero power and hot full power as defined in [8]. Three water isotopic compositions were applied – the first with H-2 and O-17, the second without O-17 and the third without O-17 and H-2. The first is the reference composition for all calculations. Water was modelled as a molecule with one oxygen atom and two hydrogen atoms with natural isotopic abundances taken from [15] and reproduced in Table 9.

Boron in the form of boric acid ($B(OH)_3$) is added to water as a soluble neutron absorber to maintain the reactor in the critical state and suppress excess reactivity. It is common practice that the boric acid in borated water is modelled only in terms of boron atoms – the $(OH)_3$ group is neglected as its concentrations are negligible.

The approach to model borated water in SERPENT was based on the BEAVRS benchmark VTT full-core inputdeck [15, 33]. As the SERPENT has the capability to mix materials, it was only necessary to provide water density, boron concentration and isotopic compositions. Boron was modelled according to its natural composition – with natural atomic fractions of B-10 (19.9%at) and B-11 (80.1%at).

Table 9.

Borated water composition properties for different core states

Borated water				
State:	HZP	HFP	HFP	COLD
Boron conc. [ppm]	1382	1184	827	0
Temperature [K]	564.82	576.55		293.15
Pressure [bar]	155.13			1.01325
Pure water density [g/cm^3]	0.7431	0.7194	0.7194	0.9982
Isotope	Atomic fraction of isotope per atom of element/molecule, [–]			
	with O-17 with H-2	without O-17 with H-2	without O-17 without H-2	
H-1	1.999688520	1.9996885200	2.0	
H-2	0.000311480	0.0003114800	0.0	
O-16	0.9996210	1.0	1.0	
O-17	0.0003790	0.0	0.0	
B-10	0.1990			
B-11	0.8010			

2.2.9. Other materials

Air was used to model gas gaps in GRCAs, RCCAs and Pyrex rods. For simplicity, its composition was defined according to [18], and it is presented in Table 10. Helium was used to model gas gaps in fuel rods and IFBAs. It consists of He-4 isotope with atomic and mass density equal to $2.4044 \cdot 10^{-4}$ [atom/b-cm] and 0.001598 [g/cm^3] respectively [15].

Table 10.

Air material card [18]

Element	Weight fraction [–]
C	0.000124
N	0.755268
O	0.231781
Ar	0.012827

2.3. Geometry

After materials definition, it was necessary to prepare core geometry. The ultimate guide to developing the full-core model is the BEAVRS PWR inputdeck published by VTT [33]. The core geometry modelling starts with 2D pins. Then they are stacked to form 3D structures like rods. In the next step, those structures are grouped into lattices to form fuel assemblies. Finally, the full core 3D model is a stack of axial cells with the main cell filled with a lattice (universe) of fuel assemblies.

2.3.1. Pins

The first and the most basic level of the core geometry are pins which are defined in the following sub-chapters.

2.3.1.1. Fuel and IFBA

There are five basic types of fuel pins in the core depending on the UO_2 enrichment. However, their geometry is the same. The fuel pin geometry is presented in Fig. 1 [8]:

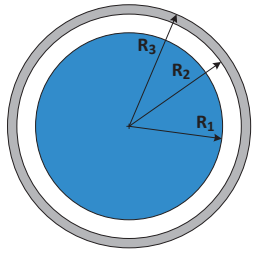

Symbol	Material	Radius [cm]
R_1	UO_2	0.409575
R_2	Helium	0.417830
R_3	ZIRLO	0.474980

Fig. 1. UO_2 fuel pin scheme

IFBA type fuel pins contain UO_2 material and an additional thin layer of ZrB_2 material (see Fig. 2). The fuel slug radius and absorbing coating thickness were assumed to be equal to 0.409595 cm and 0.00256 cm, the same values were used in Ames model [34].

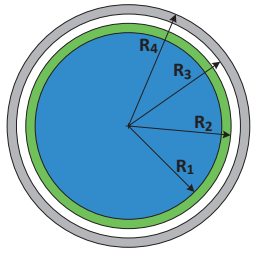

Symbol	Material	Radius [cm]
R_1	UO_2	0.409595
R_2	ZrB_2	0.412155
R_3	Helium	0.417830
R_4	ZIRLO	0.474980

Fig. 2. IFBA pin scheme

2.3.1.2. Empty Guide Tube, RCCA, GRCA and Pyrex Guide Tube

It was assumed that the geometry of the empty guide tube and instrumentation tube are the same (Fig. 3). However, their functions in the fuel assemblies are different. The guide tubes are used to introduce GRCAs or RCCAs or Pyrex rods. Instrumentation tubes are used to introduce in-core neutron detectors temporarily. In this work, it was assumed that instrumentation tubes were empty [8]. In the AP-1000 DCD [8] upper and lower part of the guide tube has slightly different geometry. For simplicity only, single geometry was applied.

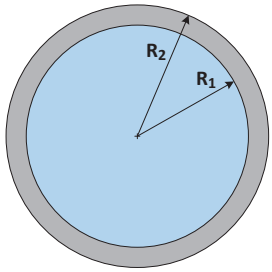

Symbol	Material	Radius [cm]
R_1	Water	0.56134
R_2	ZIRLO	0.61214

Fig. 3. Empty guide tube or instrumentation tube pin geometry

Pyrex Burnable Absorber rods are inserted into the specified guide tubes in selected fuel assemblies. The pin geometry of the Pyrex rod was based on [8] and [22], and the whole pin geometry is presented in Fig. 4.

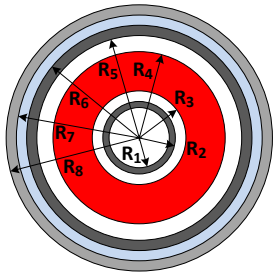

Symbol	Material	Radius [cm]
R_1	Air	0.213995
R_2	SS-304	0.230505
R_3	Air	0.241300
R_4	B_2O_3-SiO_2	0.426720
R_5	Air	0.436880
R_6	SS-304	0.483870
R_7	Water	0.561340
R_8	ZIRLO	0.612140

Fig. 4. Guide tube with the inserted Pyrex rod geometry

The RCCAs contains 24 rodlets (control rods) of Ag–In–Cd as a neutron absorber (see Fig. 7), which are inserted into reactor guide tubes when reactivity control for power operations or shutdown of the reactor is required. According to [8], the diameter of the absorber is 0.86614 cm, and the cladding material thickness is 0.04699 cm. Remaining data concerning the RCCA rod structure were taken from [23], and the geometry of the pin is presented in Fig. 5.

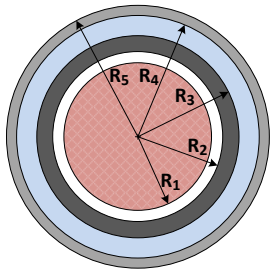

Symbol	Material	Radius [cm]
R_1	Ag-In-Cd	0.43307
R_2	Air	0.43688
R_3	SS-304	0.48387
R_4	Water	0.56134
R_5	ZIRLO	0.61214

Fig. 5. Guide tube with RCCA pin and geometry

Gray rods (GRCA) are used in load follow manoeuvring of the reactor and as a mechanical shim, to compensate for the soluble boron concentration changes. The geometry of those rods is the same as the RCCAs (see Fig. 6) except that neutron absorbing material has reduced diameter [7].

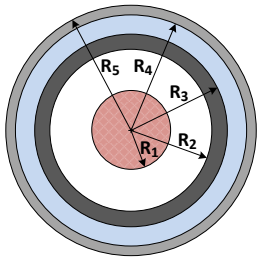

Symbol	Material	Radius [cm]
R_1	Ag-In-Cd or SS-304	0.20320
R_2	Air	0.43688
R_3	SS-304	0.48387
R_4	Water	0.56134
R_5	ZIRLO	0.61214

Fig. 6. GRCA in the guide tube geometry

2.3.2. Fuel assemblies

The higher level of the geometry is a fuel assembly. The basic geometry is presented in Fig. 7. A fuel assembly is a lattice of various combinations of fuel pins, Pyrex and IFBA rods described in Section 2.3.1. For the 1st fuel cycle, there are nine types of fuel assemblies with a standard 17×17 lattice (see Fig. 8) [8, 21, 24]. The fuel assembly has a 3D structure defined by the pin lattice, axial structure of pins and lattice boundaries (see Fig. 9).

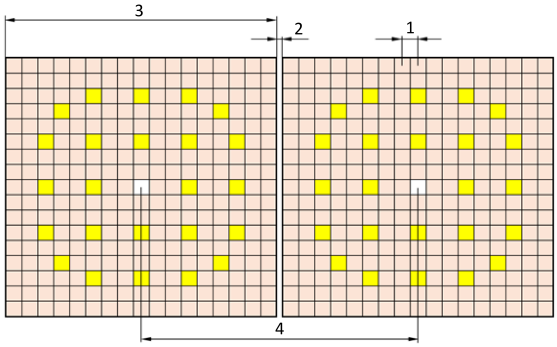

No.	Description	Dimension [cm]
1	Fuel rod pitch	1.25984
2	Space between assemblies	0.1016
3	Fuel assembly size	21.40204
4	Fuel assembly pitch	21.50364

Fig. 7. Fuel assembly geometry

The assemblies and pins are characterized by axial zoning and the different distribution of material along the length (Fig. 9). The universe with fuel assemblies lattice (and pins) extends between the top of the bottom nozzle (elevation –14.31 cm) and bottom of the top nozzle (+445.77 cm).

The fuel active core length is equal to 426.72 cm (Fig. 9) with upper and lower plenums with height 12.16/17.78 cm and end caps 1.27/2.15 cm. For Pyrex

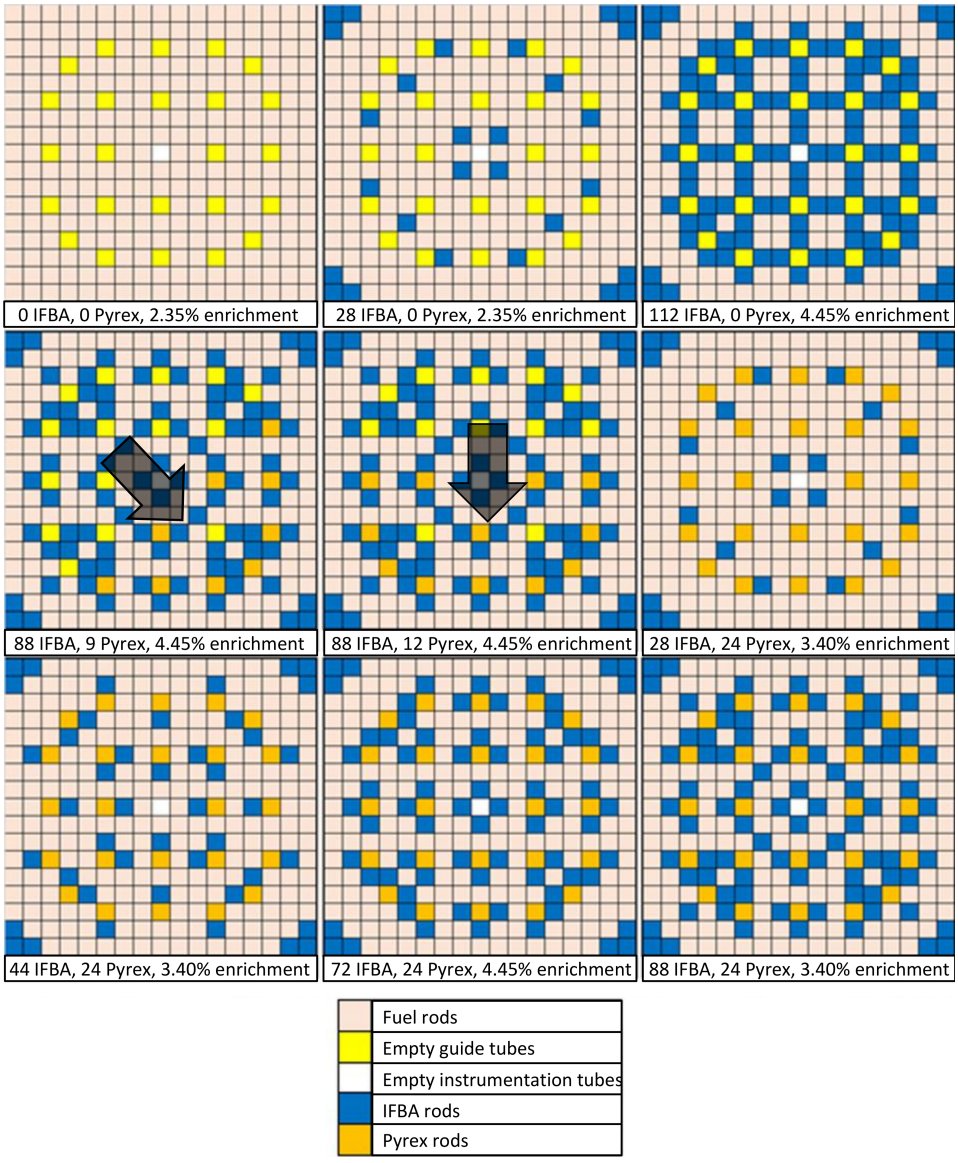

Fig. 8. Fuel assembly lattice used in the 1st fuel cycle. Transparent arrows indicate the core centre direction; based on [8, 21]

burnable absorber rods, the top and bottom 30.48 cm are filled with helium gas, whereas the middle area (368.30 cm) of the rod is made of borosilicate absorber material. For IFBA rods, the top and bottom parts of each fuel rod contain UO_2 fuel with reduced enrichment and it acts as an axial blanket for better neutron economy (20.32 cm). The central region of the IFBA rod is made of UO_2 (386.08 cm) coated with a thin layer of the ZrB_2 absorber. For a non–IFBA fuel rod, the axial blanket

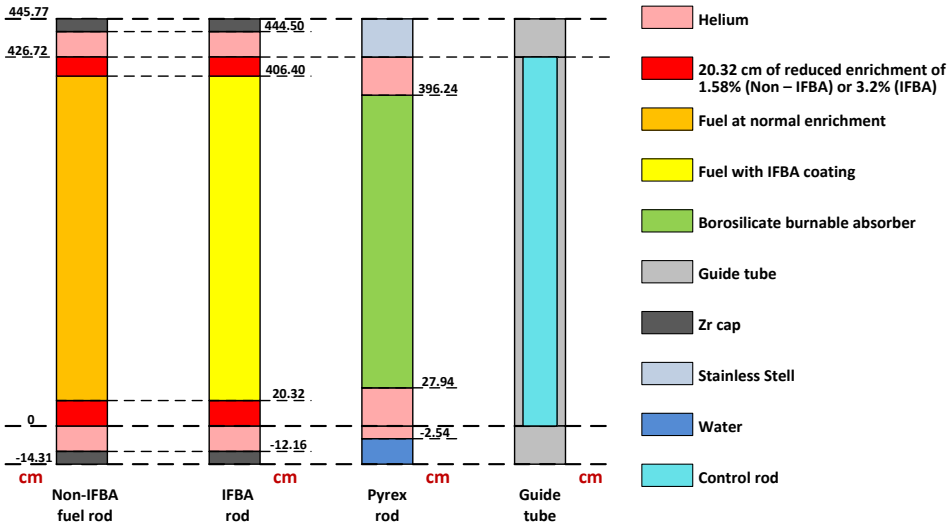

Fig. 9. Axial zoning of fuel rods, burnable absorber rods and guide tube

region contains UO_2 fuel at the enrichment of 1.58%. The remaining part of non–IFBA fuel rod contains typical enrichment [28]. All parameters were estimated based on the DCD report [5–10].

An assembly contains spacer grids which make it possible to maintain fixed distances between fuel rods and to promote mixing (Fig. 10). The AP1000 design

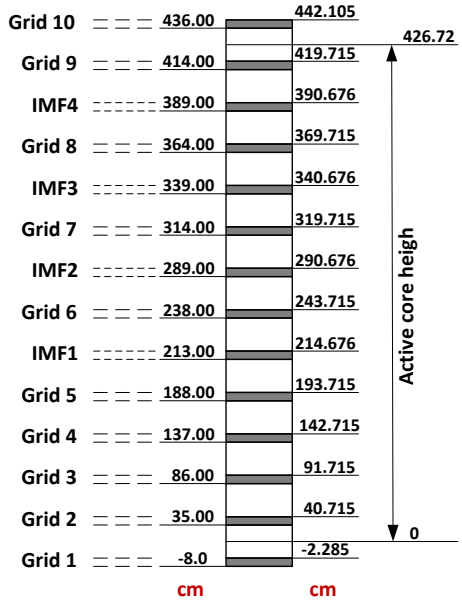

Fig. 10. Spacer grids locations

has 10 spacer grids (8 in the active part of the core) made of Zirlo alloy and 4 Intermediate Mixing Flow (IMF) grids made of Inconel-718.

The Banded Dissolution Model (BDM) was applied to model spacer grids [34]. In locations, where grids are present, water was homogeneously mixed with spacer material. Locations, volume fractions and masses of spacer grids were estimated based on the Westinghouse spacer grids description in BEAVRS [15] and DCD [5–10].

The Rod Cluster Control Assemblies (RCCA) can be divided into two categories: control and shutdown. The control groups compensate for reactivity changes due to variations in operating conditions. The Gray Rod Cluster Assemblies (GRCA) have almost identical design as RCCA, but their function is different. They are used for following the load change and provide a mechanical shim to replace the use of changes in the boron concentration. The design of RCCAs and GRCAs do not vary along the axis. The RCCAs and GRCAs are inserted only in the assemblies where all guide tubes are empty, and these are presented in the first row of Fig. 8 (0,28,112 IFBA), and RCCA rods occupy all 24 guide tubes. However, single GRCA is divided into 12 SS-304 rods and 12 Ag–In–Cd rods and is inserted into guide tubes according to the pattern presented in Fig. 11 [7].

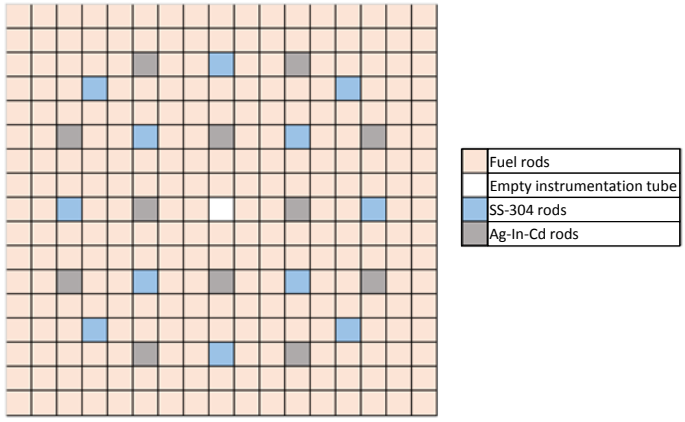

Fig. 11. GRCA typical insertion pattern in a fuel assembly [7]

2.3.3. Full-core models

The next step after fuel assemblies modelling was to prepare the whole core model. The core loading pattern of the 1st fuel cycle is presented in Fig. 12 [8, 35]. The considered core contains 157 fuel assemblies, 16 GRCAs and 53 RCCAs [5, 8, 31]. Distribution of RCCAs and GRCAs is presented in Fig. 13.

The model geometry was limited radially by the air-filled cylinder with outer radius 280 cm (Fig. 14). Axially, the model was limited by two water layers with top and bottom elevations –100 cm and +530 cm relative to the BAF (Fig. 15).

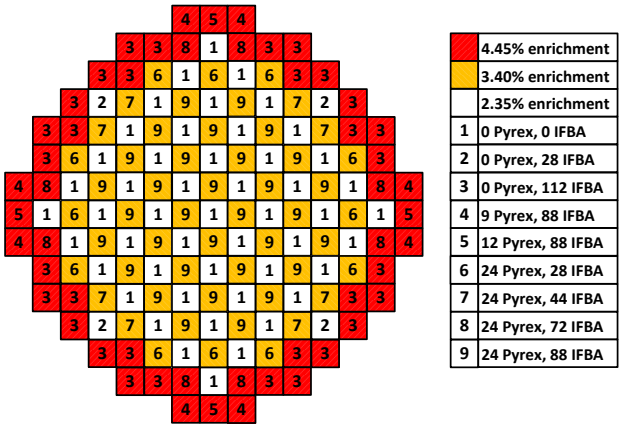

Fig. 12. Fuel enrichment distribution across core lattice for the central active core plane of rods

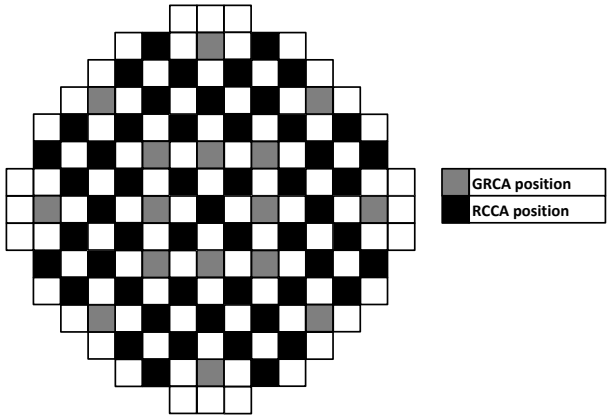

Fig. 13. Control rods assembly distribution across reactor core [8]

The RPV including core barrel and core shroud with dimensions are presented in Figs. 14 and 15. All external surfaces were set to be black boundary conditions. The core shroud material was the SS-304 steel with wall thickness 2.2225 cm [6, 28]. The core barrel was made of an SS-304 steel ring with 5.1 cm thickness [6, 28] and the RPV vessel was made of SA-508 low carbon steel ring with 20.3 cm thickness [28, 35]. In the model, those components served as neutron reflectors, and for this reason and simplicity of the geometry, all of them were modelled as rings of specified thicknesses and radii. Also, the modelled geometry did not include four neutron steel panels (pads) [36].

The basic model does not have a core baffle – as it is not described in the DCD Nuclear Design Chapter 4.3 [8]. Sensitivity calculations were performed with 1-inch (2.54 cm) thick steel baffle [37].

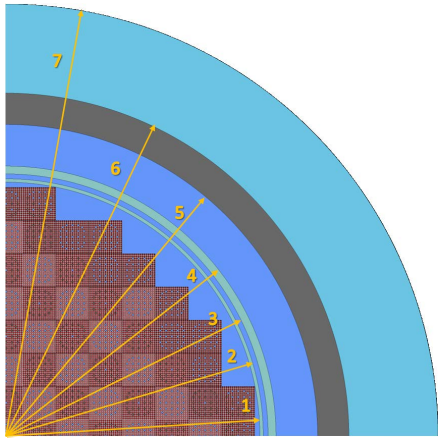

No.	Description	Dimension [cm]
1	Core shroud IR	164.531
2	Core shroud OR	166.694
3	Core barrel IR	169.863
4	Core barrel OR	174.943
5	RPV IR	201.930
6	RPV OR	222.250
7	Outer model	280.000

Fig. 14. The horizontal cross-section of the SERPENT model (quarter core) geometry with core peripherals dimensions

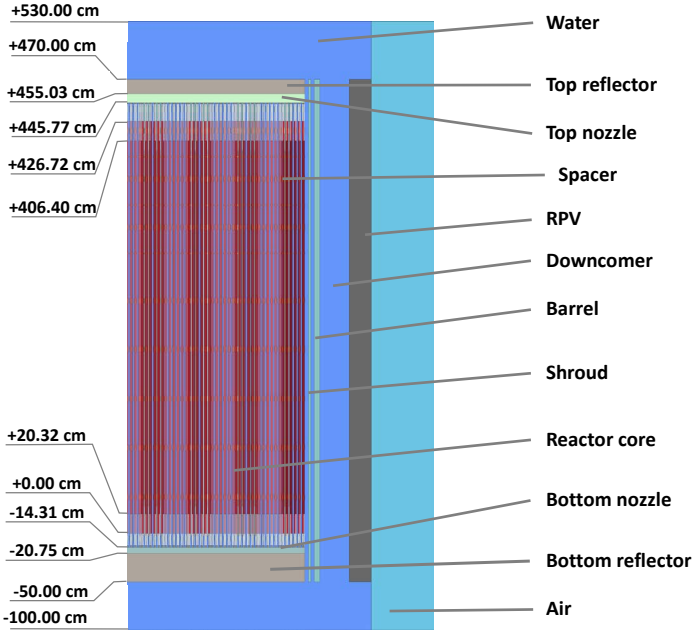

Fig. 15. The vertical cross-section (half core) of the SERPENT model

Bottom and top reflectors were modelled as homogenous mixtures of stainless steel (SS304) with water – similarly to the reflector in DCD [8]. The volume fraction of 50%/50% was assumed. Bottom and top reflectors were estimated to have 29.25 cm and 14.97 cm. Top and bottom nozzles were estimated to have heights equal to 9.26 cm and 6.44 cm, respectively, with steel volume fraction assumed to be 30%.

3. Results and discussion

3.1. Investigated cases

Simulations were prepared to verify the model by comparison with the DCD report [8]. Cold shutdown results were compared with alternative publications [20, 24, 38–40]. Several input decks for criticality calculations were prepared with different core states and sensitivity cases. Calculations were performed with recent SERPENT 2.1.29 applying ENDF/B-VII and for shutdown cases JEFF 3.1.1 to estimate the library effect [13]. Power distribution calculations were prepared with new SERPENT 2.1.30.

Cases were run with 100 million neutron histories divided into 200 active cycles with 500000 neutrons per cycle. In order to ensure fission source convergence, 225 inactive initial cycles were applied. It took about 50 cycles to converge eigenvalue and about 225 cycles to converge source (Shannon entropy). All calculations were performed with Xeon E5-2660v2 Workstation with two processors, 20 cores and 64GB RAM. Single case criticality calculation took about 2–3 hours without additional tallies. Power distributions presented in sub-chapter 3.4 were calculated for 1 billion neutrons, 2.5 million neutrons in 400 cycles and 225 inactive cycles, and a single run took about 18 h.

A single base case and eight sensitivity cases were calculated for the cold shutdown (COLD) state (Table 11). Three base cases and one sensitivity case were calculated for the Hot Zero Power (HZP) state (Table 12). Otherwise, for the Hot Full Power (HFP) state, two base cases and nine sensitivity cases were simulated (Table 12). All base cases, correspond, as far as possible, to the reference core states described in the DCD. Sensitivity cases were calculated to investigate the reactivity effects of selected parameters and to assess reactivity coefficients. Additional six cases were calculated to obtain radial power distributions in unrodded, HFP, BOL core with and without equilibrium xenon. All reactivity

Table 11.

Cold shutdown states. All COLD states have no xenon, no boron and 300 K temperature

Case	State	UO_2 TD [g/cm^3]	Spacer grids	O-17 in water	H-2 in water	O-17 in fuel	U-234 in fuel	Comment
#1	COLD	10.96	yes	yes	yes	yes	yes	Base
#2	COLD	10.96	no	yes	yes	yes	yes	Sensitivity
#3	COLD	10.96	yes	no	yes	yes	yes	Sensitivity
#4	COLD	10.96	yes	no	no	yes	yes	Sensitivity
#5	COLD	10.96	yes	no	no	no	yes	Sensitivity
#6	COLD	10.96	yes	no	no	no	no	Sensitivity
#7	COLD	10.97	yes	yes	yes	yes	yes	Sensitivity
#8	COLD	10.98	yes	yes	yes	yes	yes	Sensitivity
#9	COLD	10.96	yes	yes	yes	yes	yes	Base with baffle

Table 12.

HZP and HFP states

Case	State	Xenon	Fuel Temp. [K]	Mod. Temp. [K]	Boron [ppm]	Mod. Density [g/cm^3]	Comment
HZP							
#9	HZP	No Xe	564.8	564.8	1502	0.7431	Base
#10	HZP/CR in	No Xe	564.8	564.8	1502	0.7431	Base
#11	HZP	No Xe	564.8	564.8	1382	0.7431	Base
#12	HZP	No Xe	600.0	600.0	1502	0.7431	Sensitivity
HFP							
#13	HFP	Eq. Xe	900	576.6	827	0.7194	Base
#14	HFP	No Xe	900	576.6	1184	0.7194	Base
#15	HFP	Eq. Xe	900	600.0	827	0.7194	Sensitivity
#16	HFP	Eq. Xe	1200	576.6	827	0.7194	Sensitivity
#17	HFP	No Xe	900	600.0	1184	0.7194	Sensitivity
#18	HFP	No Xe	1200	576.6	1184	0.7194	Sensitivity
#19	HFP	No Xe	900	576.6	1184	0.7431	Sensitivity
#20	HFP	No Xe	900	564.8	1184	0.7431	Sensitivity
#21	HFP	No Xe	900	564.8	1184	0.7194	Sensitivity
#22	HFP	No Xe	900	576.6	827	0.7194	Sensitivity
#23	HFP	Eq. Xe	900	576.6	1184	0.7194	Sensitivity

differences in this document were calculated with reactivity difference formula: $\Delta\rho = (k_2 - k_1)/(k_2 k_1)10^5$ [pcm], where k_1 and k_2 are the calculated eigenvalues.

The DCD document defines the cold state as 1.01325 bar (1 atm) and 293.15 K. For this state, pure water density is equal to 0.9982 g/cm^3 (Table 11), and it is the basis of all COLD states simulated in this work. All COLD cases were calculated without xenon, with nuclear data libraries for 300 K as it is the library with the lowest temperature. They were simulated with Doppler broadening set to 300 K and the moderator thermal-scattering libraries for 293.16 K. The cold shutdown state without xenon and no boron is expected to be characterized by the highest possible core reactivity. The cold shutdown state is the primary reference case for the comparison with the DCD and other references.

In order to study the cold shutdown state, sensitivity calculations were performed for the UO_2 theoretical density (TD) with values between 10.96–10.98 g/cm^3, as it was uncertain which value was applied in the DCD. The standard value of 10.96 g/cm^3 was applied in all other code runs. What is more, sensitivity calculations were performed for the presence of minor isotopes U-234 and O-17 in the fuel and H-2, and O-17 in the moderator as concerns about their impact was raised during the research. Furthermore, it was decided to calculate all HZP and HFP cases with O-17, U-234 and H-2 present in the fuel and moderator.

The thermodynamic state with 564.82 K and 155.13 bar is defined in the DCD document as a hot state, and it corresponds to the Hot Zero Power state in this

work. The pure water density equal to 0.7431 g/cm^3 was applied in the HZP state cases (Table 12). The base calculations were performed with Doppler broadening temperature equal to 564.82 K for the fuel and all structures. Moderator thermal-scattering nuclear libraries were interpolated by SERPENT routines to 564.82 K. The single sensitivity run was performed with fuel, structure and moderator nuclear data and thermal-scattering temperature equal to 600 K entirely.

The Hot Full Power state is not directly defined in the DCD for neutronic calculations. Nevertheless, the DCD defines the core average coolant temperatures as 576.6 K and pressure 155.13 bar. The corresponding water density was estimated to be equal to 0.7194 g/cm^3. It was assumed for simplicity that temperatures and moderator densities are uniform across the core.

Sensitivity calculations were prepared for both equilibrium, and zero xenon concentrations and with boron inventory kept equal to the DCD reference values (Table 12). The fuel temperature equal to 900 K was assumed as standard value in PWR neutronic calculations, and sensitivity cases for temperature 1200 K were calculated additionally. Doppler broadening procedure was applied and moderator thermal-scattering libraries interpolation. What is essential, temperatures for core structures were equal to the coolant temperature with exceptions being fuel, Pyrex and IFBAs. Additional sensitivity cases for HFP state were calculated with increased moderator density equal to the HZP conditions, changed temperature, different moderator/structures temperatures, boron and xenon (Table 12).

3.2. Cold shutdown state results

The cold shutdown results for base and sensitivity cases are presented in Table 13. All results are within 150 pcm difference to the DCD, and majority of ENDF results are within 2–3 standard deviations (20–30 pcm) to the DCD. Obtained results can be considered as very satisfactory.

The difference between ENDF and JEFF results is relatively small, and its magnitude is less than 80 pcm. The ENDF results are higher than JEFF in all investigated cases. Otherwise, ENDF results are slightly more consistent with DCD results, and it is because the DCD results were prepared with ENDF libraries [8].

The paper [34] shows that the banded spacer grid model slightly overpredicts eigenvalue. It was shown that in a small-PWR model with banded dissolution the model overpredicts reactivity by ~100–120 pcm in comparison to the detailed heterogenous spacers model It was shown that heterogeneous model of spacers removed 420 pcm of reactivity in total. Otherwise, sensitivity calculation prepared in this work shows that banded model removes only about 80 pcm (see case #1 and #2) in comparison to the case without spacers. In consequence, obtained excellent accuracy (Table 13) can be changed slightly towards lower eigenvalues. It can be estimated that the heterogenous spacer grid model will remove ~100 pcm additionally.

Table 13.

Cold shutdown calculation results compared with the DCD

Case	ENDF				JEFF			ENDF-JEFF [pcm]
	DCD k-eff	SERPENT k-eff	Stat. Error 2SD [pcm]	Difference [pcm]	SERPENT k-eff	Stat. Error 2SD [pcm]	Difference [pcm]	
#1	1.205	1.20536	17	25	1.20434	17	–45	70
#2	1.205	1.20641	17	97	1.20545	18	31	66
#3	1.205	1.20512	20	8	1.20410	18	–62	70
#4	1.205	1.20529	17	20	1.20411	16	–61	81
#5	1.205	1.20523	16	16	1.20449	17	–35	51
#6	1.205	1.20714	18	147	1.20632	18	91	56
#7	1.205	1.20534	16	23	1.20422	18	–54	77
#8	1.205	1.20524	17	17	1.20437	16	–43	60
#9	1.205	1.20439	18	–42	–	–	–	–

The most significant difference between DCD and SERPENT was overprediction of reactivity by 147 pcm for the case (#6) without U-234. The U-234 has very low thermal fission cross-section, and absorption is comparable to U-235. Hence, it works as a neutron absorber. What is more, removing U-234 slightly changes atomic densities as average atomic mass changes.

The impact of the H-2 and O-17 in the moderator and O-17 in the fuel has the same magnitude as a 2SD statistical error (~20 pcm), and their potential influence is indistinguishable from the statistical noise. Similarly, variation in the uranium dioxide theoretical density produced the effect in the range of the error, and there is no observable effect.

The addition of 1-inch steel baffle (case #9) around the core removed ~70 pcm of reactivity. The analysis for 2D full-core of the alternative AP1000 design predicted baffle effect equal to –34 pcm [37]. A two-fold difference is probably due to the higher leakage in the investigated core design.

Table 14 presents a comparison of the cold shutdown states obtained by different researchers [20, 24, 38–40]. All calculations predicted eigenvalues with the error being less than 200 pcm. It can be observed that results presented in this work, base case and sensitivity cases are comparable to results obtained by other researchers. This remains true even considering the shift due to the spacer grids, baffle presence and eventual isotopic differences – like U-234.

It is worth emphasizing that the DCD report is not a benchmark-type detailed specification. The material definition and compositions differences are expected as all materials used in the model were calculated independently with the application of various references. A similar problem exists in the case of core geometry, some details are not specified, and there is a significant space for deviations between DCD and other studies.

Table 14.
SERPENT results in comparison with available literature for cold, zero power state with zero soluble boron at BOL

Reference	k-eff	Stat. Error 1SD [pcm]	Difference-to-DCD [pcm]
SERPENT2.1.29, base case – this work	1.20536	8	25
AP1000 DCD, Ref. [8]	1.205	N/A	–
MCNP5, Ref. [20]	1.2044	N/A	–41
SCALE/KENO-VI, Ref. [20]	1.2026	N/A	–66
MCNP5/MCNPX2.6.0, Ref. [24]	1.2039	N/A	–76
WIMS9/PARCS/TRACE, Ref. [24]	1.2038	–	–83
MCNP6, Ref. [38]	1.2045	9	–34
SERPENT, Ref. [38]	1.20421	51	–54
MCNP6, Ref. [39]	1.20403	21	–67
NODAL3 Ref. [40]	1.207	–	138

3.3. Hot Zero Power and Hot Full Power results

The Hot Zero Power (HZP) results are presented in Table 15. The base subcritical (#9) and critical (#11) cases have differences to DCD lower than 100 pcm. The sensitivity case #12 with varied temperatures underpredicts the eigenvalue by ~80pcm, the overall temperature effect is equal to –140 pcm (in comparison to case #9). The quality of results is comparable with cold shutdown studies in section 3.2. It is worth to mention that the deviation of 50 ppm of boron is considered as the industrial standard limit for neutronic criticality calculations. According to the DCD, boron coefficient design limit is between –13.5 to –5 pcm/ppm and it corresponds to reactivity limit ~250–650 pcm [8, 41, 42]. In consequence, all results for the cold shutdown state are all substantially within the minimum limit. The obtained results can be assessed as very satisfactory from the point of view of the project. It can be concluded that the boron and thermal-hydraulic modelling for HZP state is appropriate.

The DCD provides the total Control Rods Worth equal to 12690 pcm [8]. The SERPENT predicts 13340 pcm with the difference equal to 650 pcm and relative difference equal to 5.1%. The result is considered as acceptable.

The HFP results are characterized by substantially larger differences of eigenvalues in comparison to industrial limits (>250 pcm). What is important, the base case (#13) with equilibrium xenon is deviated by ~1100 pcm to the DCD, the base case without xenon (#14) by ~800pcm. The obtained difference can be affected by the boron concentration. In order to study the problem, base cases with 827 ppm and 1184 ppm of boron were recalculated with and without equilibrium xenon (#13 vs #22 and #14 vs #23, see Table 16). For the first case, it was calculated that equilibrium xenon removes ~2800 pcm and for the second case it was ~2850 pcm. It shows that the boron effect on the xenon worth is small in this case. Therefore,

Table 15.

Hot Zero Power and Hot Full Power cases result compared with the DCD

Case	DCD k-eff	SERPENT k-eff	Stat. Error 2SD [pcm]	Difference [pcm]
HZP				
#9	0.99	0.99061	26	62
#10	N/A	0.87498	94	N/A
#11	1.0	1.00093	24	93
#12	0.99	0.98924	26	–78
HFP				
#13	1.0	1.01109	26	1097
#14	1.0	1.00839	26	832
#15	1.0	1.01091	26	1079
#16	1.0	1.00481	24	479
#17	1.0	1.00800	26	794
#18	1.0	1.00197	26	197
#19	1.0	1.00967	26	958
#20	1.0	1.00995	26	985
#21	1.0	1.00846	24	839
#22	–	1.04113	23	–
#23	–	0.98072	27	–

if the boron influence is small, the fact that the clean core (no xenon) overpredicts (~800 pcm) eigenvalue suggest that the primary reason is not due to the xenon spatial effects. We can estimate that the xenon spatial effect can be up to 300 pcm.

It is worth to mention that the DCD does not provides xenon reactivity but the obtained value is consistent with available Westinghouse PWR manual report (~2900 pcm) [43].

What is also interesting, SERPENT xenon equilibrium model does not account for Sm-149. The DCD results were also obtained for the core without samarium [8]. Samarium removes ~650 pcm in equilibrium and it is independent of the neutron flux [43].

The discussion of xenon effects and comparison of the HZP with HFP suggests that the observed differences are due to the Thermal-Hydraulics (TH) modelling. Simplification was assumed that all TH parameters are uniform. It is different than in the real reactor case where temperature variations are present in the core. Moreover, coolant is characterized by axial and radial density profile. All those parameters influence power/flux distributions, boron concentration and xenon distributions. Summing up, all reactivity effects, in principle, can be responsible for the observed difference. Short quantitative discussion of selected effects is presented below. For completeness, significant reactivity coefficients were assessed for HFP state and are presented in Table 16.

Table 16.
Selected safety parameters compared with DCD. All coefficients (except control rods) are for HFP state

Parameter	SERPENT	DCD best estimate	DCD design limit	Cases
Doppler coefficeint with Eq. Xe, [pcm/K]	–2.06	–3.8 to –2.3	–6.3 to –1.8	#13 vs #16
Doppler coefficient without Xe, [pcm/K]	–2.12			#18 vs #14
Moderator Temp. Coefficient, [pcm/K]	–13.06	0 to –63	0 to –72	#20 vs #14
Boron coefficient with Eq. Xe, [pcm/ppm]	–8.58	–10.5 to –6.9	–13.5 to –5.0	#13 vs #23
Boron coefficient without Xe, [pcm/ppm]	–8.74			#14 vs #22
Control Rodw Worth, [pcm]	–13340	–12690	N/A	#9 vs #10
Equilibrium Xenon Worth, [pcm]	–2798	N/A	N/A	#14 vs #23
	–2853			#13 vs #22

The case #18 with fuel temperature raised to 1200 K is the only which is within the industrial limit, with a difference of only 200 pcm to the DCD. This case shows how significant the Doppler effect is – it removed almost 600 pcm. The obtained Doppler reactivity coefficients are within DCD best estimate limits for both equilibrium xenon and clean core.

Comparing cases #20–14 and #14–19, we can observe that changing the uniform moderator density and temperature from HZP to HFP value removes only about ~150 pcm. Predicted Moderator Temperature Coefficient is within best estimate DCD values. What is more, studying case #14–17 and #13–15 we can find that the impact of the moderator ("only") temperature variation is < 40 pcm.

Furthermore, we can assess boron reactivity effect (Table 16). The observed negative reactivity effect is ~3000 pcm. Calculated boron coefficients are within DCD best estimate limits [8].

Calculations reported above were performed for assembly-wise Automated Burunup Sequence. Additional calculations, not reported here but applied in next section, were performed for SERPENT standard xenon equilibrium modelling. The obtained eigenvalues were within 3SD.

3.4. Power density distribution

Despite differences between HFP results and DCD, it was decided to study power distributions. Fig. 16 presents the comparison of the axially averaged radial power distributions in 1/8th core symmetry [8]. The calculations were performed for the BOL state, without control rods for equilibrium xenon and no xenon. The SERPENT 2.1.30 was applied with standard equilibrium xenon setup and with assembly-wise Automated Burnup Sequence (ABS) for equilibrium xenon calculations. All power profiles are loaded with a relative statistical error lower than 0.0015.

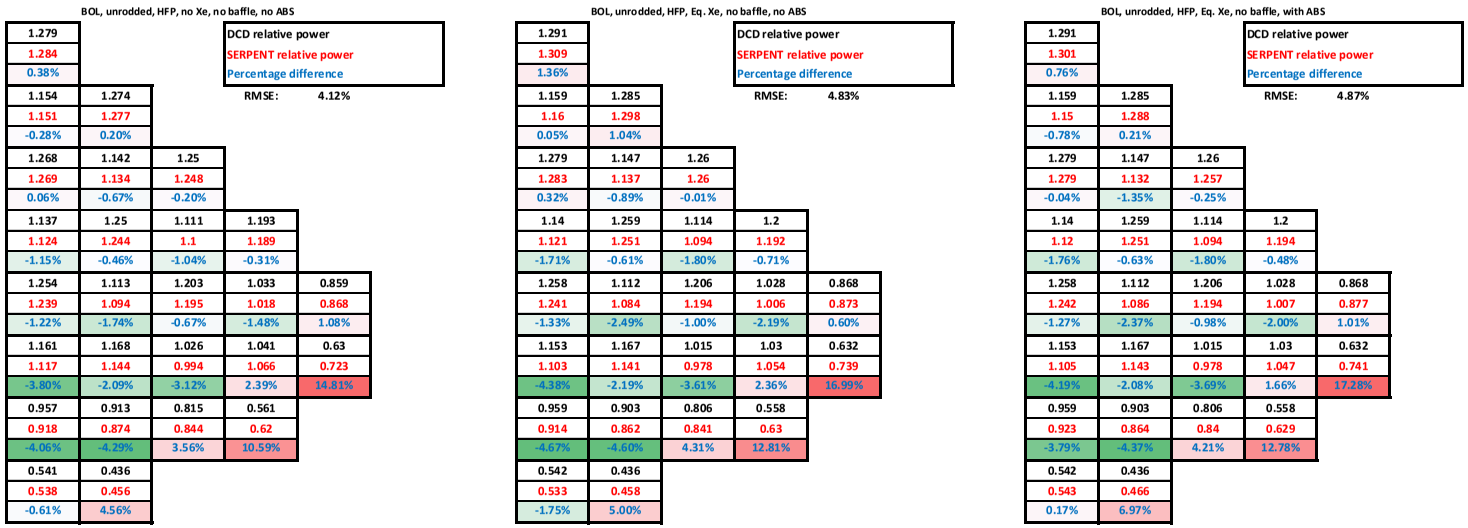

Fig. 16. Radial power distribution without the baffle; left – clean core, center – standard equilibrium xenon, right – equilibrium xenon with Automated Burnup Sequence

The Root Mean Squared Error (RMSE) of the normalized power distribution (Fig. 16) for the core without xenon is 4.1%, and for two cases with xenon, it is 4.8%. Those differences are relatively significant. What is interesting, excellent agreement was observed for central part of the core (~0.1–1.5%). Large RMSE values are mainly driven by more significant deviations at the outer regions (~5%) and large deviations (10–17%) observed in two assemblies at the core boundary.

The observed differences are probably due to the impact of the TH properties variation. Temperatures and densities are expected to be different (lower) at core boundaries, and neutronic properties will differ. Unfortunately, power profiles for the 1st cycle cold shutdown and HZP states are not available in the DCD and verification is not possible.

Differences at the core boundary suggested investigation of the reflector-type structures modelling. Radial structures: water reflector, core barrel, core shroud, downcomer and reactor vessel are consistent with available reactor design description. The only (radial) simplification applied was the removal of neutron pads, but they are located far from the assemblies characterized by significant errors. What is more, downcomer and reflector water properties were assumed to be the same as for the HFP state and it can have some impact. What is more, it is not possible to assess the impact of the axial reflector, as the axial power profile for HFP BOL was not reported in the DCD.

Report [37] investigates the AP1000 core variant with and without core baffle. The non-negligible baffle impact was discovered, and it was the motivation to test it in this work. This structure was not described in the DCD Chapter 4.3 [8], and reference results were "probably" obtained for the core without baffle – it was not confirmed. Nevertheless, power profiles were recalculated with the addition of baffle at the core boundary.

Results are presented in Fig. 17. It was observed that the presence of the baffle reduced RMSE substantially and the maximum relative power deviation is 7% for the xenon case without ABS. Nevertheless, the presence of baffle changed the neutron distribution, and more significant differences are present in the inner region of the core ~1–4%. The clean core has RMSE 2.4%, no ABS 3.3% and ABS case have RMSE equal to 2.8%. Nevertheless, the reduction of the RMSE does not provide an argument to assess those results as better than for the case without the baffle. What is also interesting, it can be observed that the calculations with equilibrium xenon are loaded with more substantial deviation to DCD.

The state-of-the-art comparison between SERPENT and ARES nodal-diffusion code for the PWR benchmark is available in [44]. The calculations showed relative differences for radial power with magnitude up to 3.5% at the core boundary and –1% in the core centre [44]. Their models were created based on the very detailed benchmark specification with small room for interpretation. Although their approach is more detailed and appropriate than the comparison presented in this work, they found relative power error as large as 3.5%.

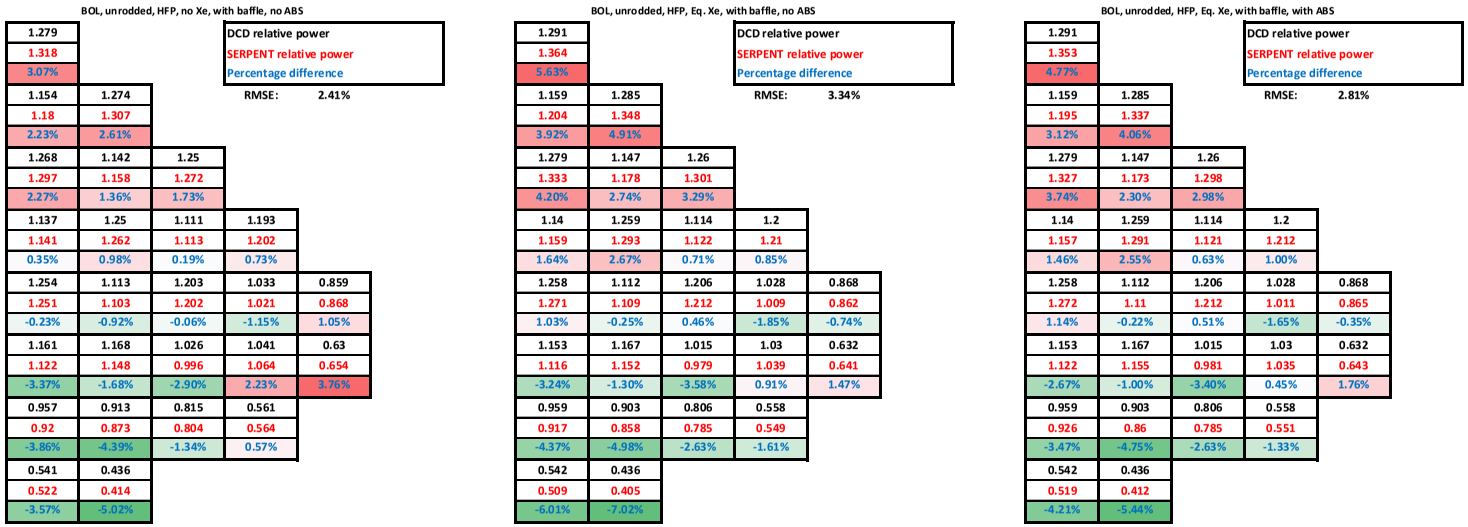

Fig. 17. Radial power distribution for core model with 1-inch baffle; left – clean core, center – standard equilibrium xenon, right – equilibrium xenon with Automated Burnup Sequence

4. Conclusions

The primary objective of this work was to develop the 3D full-core SERPENT model based on the AP1000 design and benchmark it with the publicly available documentation. The results, concerning different reactor physics parameters, were obtained, discussed and compared with DCD and other references.

In general, an excellent agreement for the Cold Shutdown and Hot Zero Power states was obtained with reactivity differences to DCD being less than 100 pcm. The results are comparable or even better than other publicly available calculations. In consequence, it can be concluded that the primary task of the research was completed successfully.

Unfortunately, the obtained Hot Full Power results are characterized by 800-1000 pcm deviation to the DCD, and it is relatively large. What is more, the obtained power distributions are acceptable for inner part of the core but diverge at the core periphery. The eigenvalue and power profile deviations are anticipated to be caused, mainly, by the assumption of uniform thermal-hydraulic conditions. The core non-uniformities are affecting the power/flux distribution, Doppler effect, moderator effect, boron and xenon effects. It shows that uniform TH modelling is not appropriate to model the Hot Full Power state. What is very interesting, all calculated reactivity coefficients (Doppler, boron and moderator) were within best estimate limits for the AP1000 design.

The model refinement can be considered in the future research. The next step is to study the impact of non-uniformities and reflector effects. It is recommended to use TH solver to predict the thermal-hydraulic state of the core and transfer it to the Monte Carlo model. Alternatively, the current practice is to use proper core simulators (i.e., nodal diffusion) with TH solvers (like PARCS/PATHS, SIMULATE, KRONOS or ARES). The presented model has a potentially wide range of applications, and it can be used to study different large Gen-III PWR core physics phenomena.

Acknowledgements

We would like genuinely to acknowledge Jaakko Leppänen and VTT Team for the creation of the excellent SERPENT computer code. We would like to state no conflict of interest with any company, organization and institution. This research was performed as an independent University's research activity and was not financed by any organization. The activates of the first author were financed by the Faculty of Power and Aeronautical Engineering Dean Grant number 504/03264 (2017).

Manuscript received by Editorial Board, November 02, 2017;
final version, July 11, 2018.

References

[1] World Nuclear Association. World Nuclear Power Reactors & Uranium Requirements. Access: 15-10-2017. http://world-nuclear.org/information-library/facts-and-figures/world-nuclear-power-reactors-and-uranium-requireme.aspx.

[2] World Nuclear Association. Nuclear Power in the World Today. Access: 15-10-2017. http://www.world-nuclear.org/information-library/current-and-future-generation/nuclear-power-in-the-world-today.aspx.

[3] International Energy Agency. International Energy Outlook 2016 (IEO2016). Access: 15-10-2017. https://www.eia.gov/outlooks/ieo/pdf/electricity.pdf.

[4] Polish Information and Foreign Investment Agency. Polish Power Sector. Access: 17.03.2017. http://www.paiz.gov.pl/files/?id_plik=19609 (in Polish).

[5] United States Nuclear Regulatory Commission. Westinghouse AP1000 Design Control Document Rev. 19, 2011. http://pbadupws.nrc.gov/docs/ML1117/ML11171A500.html.

[6] United States Nuclear Regulatory Commission. Westinghouse AP1000 Design Control Document Rev. 19 – Tier 2 Chapter 4 – Section 4.1 Summary Description, 2011. https://www.nrc.gov/docs/ML1117/ML11171A443.pdf.

[7] United States Nuclear Regulatory Commission, Westinghouse AP1000 Design Control Document Rev. 19 – Tier 2 Chapter 4 – Section 4.2 Fuel System Design, 2011. https://www.nrc.gov/docs/ML1117/ML11171A444.pdf

[8] United States Nuclear Regulatory Commission, Westinghouse AP1000 Design Control Document Rev. 19 – Tier 2 Chapter 4 – Section 4.3 Nuclear Design, 2011. https://www.nrc.gov/docs/ML1117/ML11171A445.pdf.

[9] United States Nuclear Regulatory Commission. Westinghouse AP1000 Design Control Document Rev. 19 – Tier 2 Chapter 4 – Section 4.4 Thermal and Hydraulic Design, 2011. https://www.nrc.gov/docs/ML1117/ML11171A446.pdf.

[10] United States Nuclear Regulatory Commission, Westinghouse AP1000 Design Control Document Rev. 19 – Tier 2 Chapter 4 – Section 4.5 Reactor Materials, 2011. https://www.nrc.gov/docs/ML1117/ML11171A447.pdf.

[11] Westinghouse, AP1000 nuclear power plant overview, February 2016. http://www.westinghousenuclear.com/New-Plants/AP1000-PWR/Overview.

[12] J. Leppänen. *Development of a New Monte Carlo Reactor Physics Code*. D.Sc. Dissertation, Helsinki University of Technology, Espoo, Finland, 2007.

[13] J. Leppänen. *Serpent – a Continuous-energy Monte Carlo Reactor Physics Burnup Calculation Code*. Code Manual, VTT Technical Research Centre of Finland, 18 June, 2015.

[14] J. Leppänen, M. Pusa, T. Viitanen, V. Valtavirta, and T. Kaltiaisenaho. The Serpent Monte Carlo code: Status, development and applications in 2013. *Annals of Nuclear Energy*, 82:142–150, 2015. doi: 10.1016/j.anucene.2014.08.024.

[15] MIT Computational Reactor Physics Group. BEAVRS – Benchmark for Evaluation Reactor Validation of And Simulations Rev. 2.0.1. 2017.

[16] C.D. Harmon, R.D. Busch, J.F. Briesmeister, R.A. Forster. Criticality Calculations with MCNP5™ – A Primer Appendix B: Calculating Atom Densities. Los Alamos National Laboratory Technical Manual, 1994. https://www.osti.gov/servlets/purl/10171566.

[17] Nuclear Energy Agency. NEA-1854 ZZ-SERPENT117-ACELIB, February 2016. http://www.oecd-nea.org/tools/abstract/detail/nea-1854.

[18] Pacific Northwest National Laboratory, Compendium of Material Composition Data for Radiation Transport Modeling, 2011, http://www.pnnl.gov/main/publications/external/technical_reports/PNNL-15870Rev1.pdf.

[19] D. Vollath. Uranium Dioxide, UO_2 Mechanical and Thermal Properties. Chapter 4, in: V. Haase, H. Keller-Rudek. *U Uranium: Suplement Volume C5 Uranium Dioxide UO_2 Physical Properties. Electrochemical Behavior of Gmelin Handbook of Inorganic Chemistry*, Springer, 1986. https://www.springer.com/gp/book/9783540935247.

[20] D.E. Ames. *High-fidelity nuclear energy system optimization towards an environmentally benign, sustainable, and secure energy source*. Ph.D. Thesis, Texas A&M University, College Station, USA, 2010.

[21] S. Pramuditya. *Integral Fuel Burnable Absorber (IFBA): Atomic number density calculation*. Technical discussion, 2009. https://syeilendrapramuditya.wordpress.com/2009/12/05/integral-fuel-burnable-absorber-ifba-atomic-number-density-calculation.

[22] J.C. Wagner and C.V Parks. Parametric study of the effect of burnable poison rods for PWR burnup credit. Technical Report. Oak Ridge National Laboratory, Sept. 2001. doi: 10.2172/814219.

[23] International Atomic Energy Agency. Control assembly materials for water reactors: Experience, performance and perspectives. Technical Report, 2000. http://www-pub.iaea.org/MTCD/publications/PDF/te_1132_prn.pdf.

[24] M.A. Elsawi and A.S. Bin Hraiz. Benchmarking of the WIMS9/PARCS/TRACE code system for neutronic calculations of the Westinghouse AP1000^{TM} reactor. *Nuclear Engineering and Design*, 293:249–257, 2015. doi: 10.1016/j.nucengdes.2015.08.008.

[25] Westinghouse. Optimized ZIRLO™. Report: WCAP-14342-A & CENPD-404-NP-A, Westinghouse Non-Proprietary Class 3, Addendum 1-A, 2006. http://pbadupws.nrc.gov/docs/ML0620/ML062080569.pdf.

[26] S.M. Bragg-Sitton. Light Water Reactor Sustainability Program. Advanced LWR Nuclear Fuel Cladding System Development Technical Program Plan. Idaho National Laboratory, December 2012. https://lwrs.inl.gov/Advanced%20Light%20Water%20%20Nuclear%20Fuels/AdvLWRNucFuelCladdingSys_TPP_December2012.pdf.

[27] M. Billone, Y. Yan, and T. Burtseva. LOCA embrittlement test results for high-burnup cladding. USNRC Regulatory Information Conference, Rockville, MD, USA, March 12, 2008. http://www.nrc.gov/public-involve/conference-symposia/ric/past/2008/slides/billone.pdf.

[28] B.N. Burgos. LWR Materials for Commercial Nuclear Power Applications. ATR National Scientific User Facility, June 9, 2010. https://nsuf.inl.gov/Documents/BurgosINLTalkRevMay252010Complete.pdf.

[29] United States Nuclear Regulatory Commission. Westinghouse AP1000 Design Control Document Rev. 19 – Tier 2 Chapter 5 – Section 5.2 Integrity of Reactor Coolant Pressure Boundary, 2011. https://www.nrc.gov/docs/ML1117/ML11171A451.pdf.

[30] *Carbon Steel Handbook*. Electric Power Research Institute, Palo Alto, CA, 2007. 1014670. http://www.uobabylon.edu.iq/eprints/publication_12_18692_70.pdf.

[31] Y.M. Cheong, J.H. Kim, J.H. Hong, and H.K. Jung. Dynamic elastic constants of weld HAZ of SA 508 CL.3 steel using resonant ultrasound spectroscopy. *15th World Conference on Nondestructive Testing*, Rome, Italy, 15–21 October, 2000. https://www.ndt.net/article/wcndt00/papers/idn432/idn432.htm.

[32] M. Holmgren. X-Steam Steam Tables for MATLAB. https://www.mathworks.com/matlabcentral/fileexchange/9817-x-steam-thermodynamic-properties-of-water-and-steam, 2007.

[33] J. Leppanen, R. Mattila, and M. Pusa. Validation of the SERPENT-Ares code sequence using the MIT BEAVRS benchmark – Initial core at HZP conditions. *Annals of Nuclear Energy*, 69:212–225, 2014. doi: 10.1016/j.anucene.2014.02.014.

[34] X.E. Tran and N.Z. Cho. A study of neutronics effects of the spacer grids in a typical PWR via Monte Carlo calculation. *Nuclear Engineering and Technology*, 48(1):33–42, 2016. doi: 10.1016/j.net.2015.10.001.

[35] International Atomic Energy Agency. Status report 81 – Advanced Passive PWR (AP 1000), 2011. https://aris.iaea.org/PDF/AP1000.pdf.

[36] F. Franceschini, A.T. Godfrey, and J.C. Gehin. AP1000 PWR Reactor Physics Analysis with VERA-CS and KENO-VI – Part I: Zero Power Physics Tests. *Proceedings of the International Conference on Physics of Reactors (Physor 2014)*. Kyoto, Japan, Sept. 28 – Oct. 3, 2014. https://aris.iaea.org/PDF/AP1000.pdf.

[37] F. Franceschini, A. Godfrey, J. Kulesza, and R. Oelrich. Westinghouse VERA Test Stand – Zero Power Physics Test Simulations for the AP1000 PWR. Report CASL-U-2014-0012-000, 2014. https://www.casl.gov/sites/default/files/docs/CASL-U-2014-0012-001.pdf.

[38] G.L. Stefani, P.R. Rossi, J.R. Maiorino, and T.A. Santos. Neutronic and thermal-hydraulic calculations for the AP-1000 NPP with the MCNP6 and SERPENT codes. *2015 International Nuclear Atlantic Conference – INAC 2015*, Sao Paulo, SP, Brazil, 4-9 October, 2015. http://www.iaea.org/inis/collection/NCLCollectionStore/_Public/46/133/46133779.pdf.

[39] R F. Mahmoud, M.K. Shaat, S.A.M. Agamy, and M.E-S. Nagy. Modeling and Validation of an Advanced Pressurized Water Reactor using Monte Carlo Technique. The International Journal of Science & Technoledge, 5(9):11–28, 2017. http://www.theijst.com/wp-content/uploads/2017/10/2.-ST1709-023.pdf, 2017.

[40] S. Pinem, T.M. Sembiring, T. Deswandri, and G.R. Sunaryo. Reactivity coefficient calculations for AP1000 reactor using the NODAL3 code. *Journal of Physics: Conf. Series* 962:012057, 2018. doi: 10.1088/1742-6596/962/1/012057.

[41] A.L. Nigro and F.D'Auria. PWR core response to boron dilution transient. *Proceedings of International Conference Nuclear Energy for New Europe 2003*, Portorož, Slovenia, September 8–11, 2003. http://193.2.7.48/proc/port2003/pdf/219.pdf.

[42] New York Power. Indian Point 3 Nuclear Power Plant – Cycle 11 Physics Test Report, IPN-00-004. https://www.nrc.gov/docs/ML0036/ML003679481.pdf, 18.01.2000.

[43] Westinghouse Technology Systems Manual – Section 2.1 Reactor Physics Review, 2008. https://www.nrc.gov/docs/ML1122/ML11223A207.pdf.

[44] J. Leppanen and R. Mattila. Validation of the Serpent-ARES code sequence using the MIT BEAVRS benchmark – HFP conditions and fuel cycle 1 simulations. *Annals of Nuclear Energy*, 96:324–331, 2016. doi: 10.1016/j.anucene.2016.06.014.